Proceedings of the
44th IEEE Conference on Decision and Control, and
the European Control Conference 2005
Seville, Spain, December 12-15, 2005

Observability matrix and parameter identification: application to vehicle tire cornering stiffness

Joanny Stéphant and Ali Charara

Abstract— **Tire cornering stiffness is an important parameter of vehicle modeling. Together with sideslip angle it is a transversal force governing tire-road contact, and like sideslip angle it can be used to evaluate lateral vehicle stability. This paper presents a vehicle sideslip angle observer based on a nonlinear vehicle model. This observer is validated with experimental data. Using the properties of the observability matrix, the paper shows that tire cornering stiffness is identifiable from the singular values of this matrix. An identification procedure is performed, by simulation, with double lane-change tests. Th results of this identification are validated on a slalom test. The study is carried out using a realistic vehicle simulator.**

I. INTRODUCTION

A vehicle is a highly complex system bringing together a large number of mechanical, electronic and electromechanical elements. To describe all the movements of the vehicle, numerous measurements and a precise mathematical model are required.

In vehicle development, knowledge of wheel-ground contact forces is important. This information is useful for security actuators, for validating vehicle simulators and for advanced vehicle control systems.

Braking and control systems must be able to stabilize the car during cornering. When subject to transversal forces, such as when cornering, or in the presence of a camber angle, tire torsional flexibility produces an aligning torque which modifies the original wheel direction. The difference is characterized by an angle known as ”sideslip angle”. This is a significant signal in determining the stability of the vehicle [1], and it is the main transversal force variable. Measuring sideslip angle would represent a disproportionate cost in the case of an ordinary car, and it must therefore be observed or estimated [2] and [3].

The aim of an observer or virtual sensor is to estimate a particular unmeasurable variable from available measurements and a system model. This is an algorithm which describes the movement of the unmeasurable variable by means of statistical conclusions from the measured inputs and outputs of the system. This algorithm is applicable only if the system is observable. System observability can be defined using Lie derivative theory [4].

In [5], different observers of vehicle sideslip angle are evaluated (Luenberger Observer, Extended Kalman Filter and Sliding mode observer). Together with [6] it shows a link between the condition number of the observability matrix and certain vehicle parameters or variables. One of these parameters is tire cornering stiffness. This parameter is essential in the evaluation of the potential of tires used. A tire in total sideslip presents a null cornering stiffness. Knowledge of this parameter is also useful in the evaluation of a vehicle’s lateral stability potential.

Identification theory is perfectly parallel to observation theory [7]. In this paper, a tire cornering stiffness identification is performed using a singular value of the observability matrix. First, a nonlinear vehicle model is presented, and its assumptions listed. A vehicle sideslip angle sliding mode observer is then proposed and validated on experimental data acquired with the Heudiasyc Laboratory experimental vehicle. By studying the observability properties of the observer, the paper presents the relation between the observability matrix condition number and variations in tire cornering stiffness. This part of our work uses a realistic vehicle simulator as a reference. Because of the condition number definition, a singular value decomposition of the observability matrix is performed. This decomposition shows the link between variations in real tire cornering stiffness and variations in the smallest singular value. The relation is identified using least mean squares and several double lane-change tests. Finally, identified relation is evaluated and validated using a slalom test.

II. NONLINEAR VEHICLE MODEL

Lateral vehicle dynamics has been studied since the 1950s. In 1956 Segel [8] presented a vehicle model with three degrees of freedom in order to describe lateral movements including roll and yaw. If roll movement is ignored, a simple model known as the ”bicycle model” is obtained. This model is currently used for studies of lateral vehicle dynamics (yaw, lateral speed and sideslip). A nonlinear representation of the bicycle model is shown in Fig. 1. Notations are explained in section VIII.

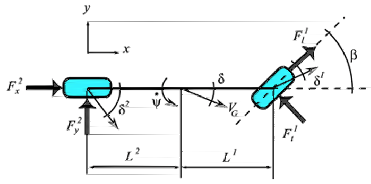

Fig. 1. Nonlinear bicycle model

Certain simplifications are used in this study. Cornering

J. Stéphant and A. Charara are with HEUDIASYC Laboratory (UMR CNRS UTC 6599) - Centre de Recherches de Royallieu BP20529 - 60205 COMPIEGNE cedex France joanny.stephant@hds.utc.fr ; ali.charara@hds.utc.fr

Thanks to SERA-CD company (http://www.sera-cd.com)

Thanks to Pr. D. Meizel - GERME - ENSIL - 16 rue Atlantis Parc d’Ester Technopole BP 6804 - 87068 LIMOGES cedex, France

0-7803-9568-9/05/$20.00 ©2005 IEEE

stiffness is taken to be constant. But cornering stiffness is modified by vertical forces on the wheel. Variations in cornering stiffness during the course of a double lane change at 90km/h are shown in Fig. 7.

Tire-road forces are highly nonlinear. Various wheel-ground contact force models are to be found in the literature, including a comparison between three different models in [5]. In this paper, transversal forces are taken to be linear. This assumption is reasonable, given that when lateral acceleration of the vehicle is less than $0.4g$ [9], transversal forces on the tires are in the linear section of the curve (Fig. 2). Consequently, transversal forces can be written as:

$$F_y^i = C_{F\delta}^i . \delta^i \quad i = 1, 2 \tag{1}$$

Rear and front tire sideslip angles are calculated as:

$$\begin{cases} \delta^1 &= \beta - \delta - L^1 \dfrac{\dot{\psi}}{V_G} & \text{(2a)} \\ \delta^2 &= -\delta + L^2 \dfrac{\dot{\psi}}{V_G} & \text{(2b)} \end{cases}$$

The vehicle model can be expressed in terms of a nonlinear state space formulation as follows:

$$\begin{cases} \dot{\mathbf{x}} &= \mathbf{f}_{MNL}(\mathbf{x}, \mathbf{u}) \\ \mathbf{z} &= \mathbf{h}_{MNL}(\mathbf{x}, \mathbf{u}) \end{cases} \tag{3}$$

State, control and measurement variables are defined as :

$$\begin{cases} \mathbf{x} &= \begin{pmatrix} V_G & \delta & \dot{\psi} \end{pmatrix}^T & \text{(4a)} \\ \mathbf{u} &= \begin{pmatrix} \beta & F_l^1 & F_l^2 \end{pmatrix}^T & \text{(4b)} \\ \mathbf{z} &= \left(V_G \quad \left[\ddot{y} - \dfrac{C_{F\delta}^1}{m_v} \beta \right] \right)^T & \text{(4c)} \end{cases}$$

Evolution equations $\mathbf{f}_{MNL}$ are written as :

$$\begin{cases} \dot{\mathbf{x}}_1 = & \frac{1}{m_v} \left(\mathbf{u}_2 \cos(\mathbf{x}_2 - \mathbf{u}_1 + \mathbf{u}_3 \cos(\mathbf{x}_2) \right) \\ & + \frac{1}{m_v} \left(C_{F\delta}^1 \left(\mathbf{u}_1 - \mathbf{x}_2 - L^1 \frac{\mathbf{x}_3}{\mathbf{x}_1} \right) \sin(\mathbf{x}_2 - \mathbf{u}_1) \right) \\ & + \frac{1}{m_v} C_{F\delta}^2 \left(-\mathbf{x}_2 + L^2 \frac{\mathbf{x}_3}{\mathbf{x}_1} \right) \sin(\mathbf{x}_2) \\ \dot{\mathbf{x}}_2 = & \frac{1}{m_v \mathbf{x}_1} \left(\mathbf{u}_2 \sin(\mathbf{u}_1 - \mathbf{x}_2) - \mathbf{u}_3 \sin(\mathbf{x}_2) \right) \\ & + \frac{1}{m_v \mathbf{x}_1} \left(C_{F\delta}^1 \left(\mathbf{u}_1 - \mathbf{x}_2 - L^1 \frac{\mathbf{x}_3}{\mathbf{x}_1} \right) \cos(\mathbf{u}_1 - \mathbf{x}_2) \right) \\ & + \frac{1}{m_v \mathbf{x}_1} C_{F\delta}^2 \left(-\mathbf{x}_2 + L^2 \frac{\mathbf{x}_3}{\mathbf{x}_1} \right) \cos(\mathbf{x}_2) - \mathbf{x}_3 \\ \dot{\mathbf{x}}_3 = & \frac{1}{I_{zz}} \left(L^1 \mathbf{u}_2 \sin(\mathbf{u}_1) - L^2 C_{F\delta}^2 \left(-\mathbf{x}_2 + L^2 \frac{\mathbf{x}_3}{\mathbf{x}_1} \right) \right) \\ & + \frac{1}{I_{zz}} \left(L^1 C_{F\delta}^1 \left(\mathbf{u}_1 - \mathbf{x}_2 - L^1 \frac{\mathbf{x}_3}{\mathbf{x}_1} \right) \cos(\mathbf{u}_1) \right) \end{cases}$$

and observation equations $\mathbf{h}_{MNL}$:

$$\begin{pmatrix} \mathbf{h}_{MNL}^1 \\ \mathbf{h}_{MNL}^2 \end{pmatrix} = \begin{pmatrix} \mathbf{x}_1 \\ -\frac{C_{F\delta}^1 + C_{F\delta}^2}{m_v} \mathbf{x}_2 + \frac{C_{F\delta}^2 L^2 - C_{F\delta}^1 L^1}{m_v \mathbf{x}_1} \mathbf{x}_3 \end{pmatrix}$$

III. SLIDING MODE OBSERVER - PRESENTATION AND EXPERIMENTAL VALIDATION

A. Sliding mode observer of vehicle sideslip angle

From [10] it is clear that this kind of observer is useful when working with reduced observation error dynamics and when seeking a finite time convergence for all observable states, as well as robustness when confronted with parameter variations (with respect to conditions).

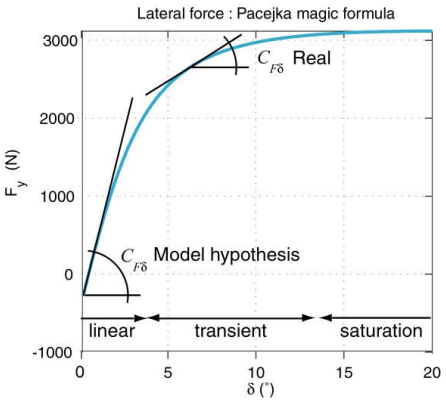

Fig. 2. Tire lateral force and cornering stiffness

A sliding mode observer applied to a nonlinear vehicle model (3) can be summarized as :

$$\begin{cases} \dot{\widehat{\mathbf{x}}} &= \mathbf{f}_{MNL}(\widehat{\mathbf{x}}, \mathbf{u}) + \mathbf{\Lambda} sign_{eq}(\mathbf{z}_2 - \widehat{\mathbf{z}}_2) & \text{(5a)} \\ \widehat{\mathbf{z}}_2 &= \begin{pmatrix} \mathbf{h}_{MNL}^1(\widehat{\mathbf{x}}) & \mathbf{h}_{MNL}^2(\widehat{\mathbf{x}}) \end{pmatrix}^T & \text{(5b)} \\ \mathbf{z}_2 &= \left(V_{Gm} \quad \left[\ddot{y}_m - \dfrac{C_{F\delta}^1}{m_v} \beta_m \right] \right)^T & \text{(5c)} \end{cases}$$

where $\mathbf{\Lambda}$ is the observer gain matrix in $\mathbb{R}^{3x2}$. To cover chattering effects, the function $sign_{eq}$ used in this paper is

$$sign_{eq}(x) = \arctan(x) * 2/\pi$$

Measures used in (5c) are available in actual vehicle.

B. Experimental vehicle

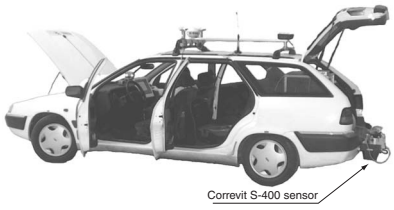

Fig. 3. Heudiasyc laboratory - Experimental vehicle: STRADA

STRADA is the Heudiasyc Laboratory's test vehicle: a Citroën Xantia station wagon equipped with number of sensors, shown in figure 3. Experimental tests described in this paper use

- GPS
- Longitudinal accelerometer
- Lateral accelerometer
- Odometry: rotational speeds of the four wheels (ABS sensors)
- Yaw rate gyrometer
- Steering angle
- Correvit Sensor

The speed of the center of gravity (V_{Gm}) is calculated as the mean of the longitudinal speeds of the two rear wheels (odometry).

The Correvit S-400 is a non-contact optical sensor mounted at the rear of STRADA on the sprung mass of the car. The S-400 Sensor provides highly accurate measurements of distance, speed and acceleration, sideslip angle, drift angle and yaw angle. The S-400 Sensor uses proven optical correlation technology to ensure the most accurate possible signal representation. This technology incorporates a high intensity light source that illuminates the test surface, which is optically detected by the sensor via a two-phase optical grating system.

C. Experimental validation of the sliding mode observer

Experimental validation of the sliding mode observer (5) was carried out over a test track circuit located at Satory - Versailles, France. The observer was tested over two laps on the track. Fig. 4 presents the GPS recording and the acceleration diagram. Throughout the experimental test the lateral acceleration remained below 0.4g, which is the limit for lateral-force linearity, given our hypothesis (1).

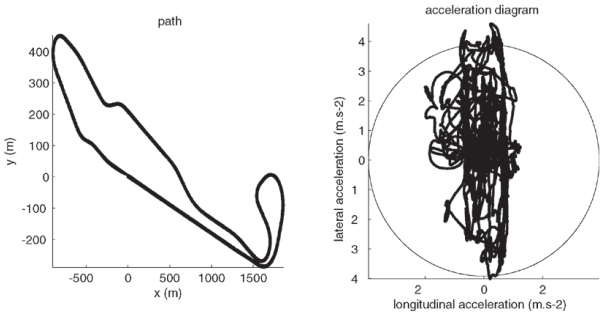

Fig. 4. Vehicle path and acceleration diagram - experimental validation

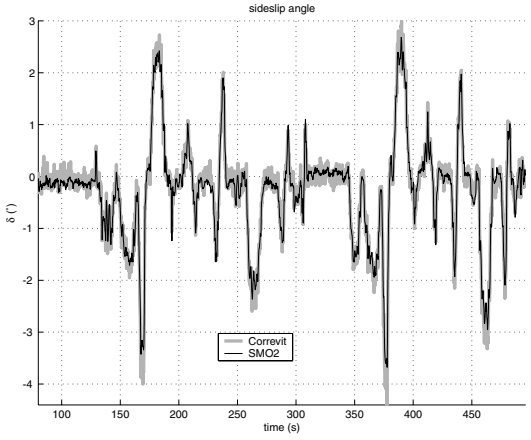

Fig. 5. Sliding mode observer for vehicle sideslip angle - experimental validation

Fig. 5 shows the good sideslip angle reconstruction obtained using observer (5). In [5] it was shown that this observer, associated with model (3) (based on hypothesis (1)) gives good results when the lateral acceleration is below 0.6g, as in this experimental test.

IV. NONLINEAR OBSERVABILITY OF THE SIDESLIP ANGLE OBSERVER

In the nonlinear state space formulation, the observability definition is local and uses the Lie derivative [4]. It is a function of state trajectory and inputs applied to the model. For the system described by equation (3) and sensor set (5c) the observability function is:

$$\mathbf{o}_2(\mathbf{x},\mathbf{u}) = \begin{pmatrix} \mathbf{h}^1(\mathbf{x}) \\ (\mathcal{L}_\mathbf{f}\mathbf{h}^1)(\mathbf{x},\mathbf{u}) \\ (\mathcal{L}^2_\mathbf{f}\mathbf{h}^1)(\mathbf{x},\mathbf{u}) \\ \mathbf{h}^2(\mathbf{x}) \\ (\mathcal{L}_\mathbf{f}\mathbf{h}^2)(\mathbf{x},\mathbf{u}) \\ (\mathcal{L}^2_\mathbf{f}\mathbf{h}^2)(\mathbf{x},\mathbf{u}) \end{pmatrix} \tag{6}$$

$$\text{with} \begin{cases} \mathcal{L}_\mathbf{f}\mathbf{h}^j(\mathbf{x}) & = \dfrac{d\mathbf{h}^j(\mathbf{x})}{d\mathbf{x}}\mathbf{f}(\mathbf{x},\mathbf{u}) & \text{(7a)} \\ \mathcal{L}^{i+1}_\mathbf{f}\mathbf{h}^j(\mathbf{x}) & = \dfrac{d\mathcal{L}^i_\mathbf{f}\mathbf{h}^j(\mathbf{x})}{d\mathbf{x}}\mathbf{f}(\mathbf{x},\mathbf{u}) & \text{(7b)} \end{cases}$$

The observability function is therefore expressed as:

$$\mathbf{o}_2 = \begin{pmatrix} \mathbf{h}^1_{MNL} \\ \mathbf{f}^1_{MNL} \\ \sum_{i=1}^{3}\left[\dfrac{\partial \mathbf{f}^1_{MNL}}{\partial \mathbf{x}_i}\right].\mathbf{f}^i_{MNL} \\ \mathbf{h}^2_{MNL} \\ \sum_{i=1}^{3}\dfrac{\partial \mathbf{h}^2_{MNL}}{\partial \mathbf{x}_i}.\mathbf{f}^i_{MNL} \\ \sum_{i=1}^{3}\dfrac{\partial}{\partial \mathbf{x}_i}\left[\sum_{i=1}^{3}\dfrac{\partial \mathbf{h}^2_{MNL}}{\partial \mathbf{x}_i}.\mathbf{f}^i_{MNL}\right].\mathbf{f}^i_{MNL} \end{pmatrix} \tag{8}$$

If the $\mathbf{o}_2$ function is invertible at the current state and input, the system is observable. This function is invertible if its Jacobian matrix $\mathcal{O}_2$ has a full rank. This "Observability matrix" is defined as:

$$\mathcal{O}_2 = \frac{d}{d\mathbf{x}}\mathbf{o}_2(\mathbf{x},\mathbf{u}) \tag{9}$$

V. SIMULATION CONDITIONS

A. Callas Simulator

The Callas simulator provides simulations which can be used to study the performance of the sliding mode observer of vehicle sideslip angle. This software is a realistic simulator validated by car manufacturers and research institutions including INRETS ("Institut national de recherche sur les transports et leur sécurité"). The Callas model takes into account vertical dynamics (suspension, tires), kinematics, elasto-kinematics, tire adhesion and aerodynamics. This vehicle simulator was developed by the SERA-CD company.

B. Simulation path: double lane change

Sideslip angle is the most important variable used when calculating tire-road transversal forces and studying the lateral stability of a vehicle. The performance of the observer is evaluated on an ISO double lane change (Fig. 6). This kind of test is representative of the transient lateral behavior of a vehicle. The double lane change is performed at 90km/h in

order to reveal links between observability singular values and tire cornering stiffness.

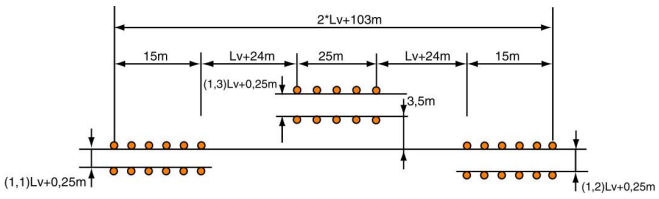

Fig. 6. Double lane-change ISO

C. Tire cornering stiffness

Tire cornering stiffness, as calculated by the Callas simulator, is defined as

$$C_{F\delta}^{Callas} = \frac{\partial}{\partial \delta} F_y^P(g_l, \delta, c, F_z) \tag{10}$$

where lateral force F_y^{P1} is calculated by Pacejka's "magic formula" using sixty parameters to characterize longitudinal, transversal and self-aligning torque of the tire-road contact [11]. Fig. 7 presents the inverse of cornering stiffness obtained from the Callas Simulator for a double lane change at 90km/h.

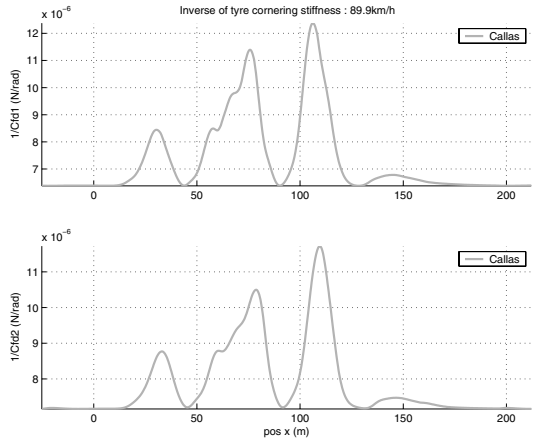

Fig. 7. Inverse of tire cornering stiffness - double lane change (90km/h)

VI. IDENTIFICATION OF TIRE CORNERING STIFFNESS USING THE OBSERVABILITY MATRIX

[6] presents the relation between condition number and the observability matrix. Available measurements were the speed of the center of gravity V_G and the yaw rate $\dot{\psi}$. An equivalent logic can be used for measurement set (5c).

Fig. 8 shows variations in the condition number of $\mathcal{O}_2$ for a double lane change at 90km/h. This condition number is calculated at each time step at the local observed state. The main value for the condition number is directly linked to the vehicle's speed as it crosses an obstacle. But variations in the condition number is related to variations in tire cornering stiffness (Fig. 7). These results indicate the necessity for an analysis of singular values of the observability matrix. Indeed, the 2-Norm condition number of the observability matrix is the ratio of the largest singular value of $\mathcal{O}_2$ to the smallest:

$$cond(\mathcal{O}_2) = \frac{\lambda_{max}}{\lambda_{min}} \tag{11}$$

[1]This formulation included coupling between longitudinal and transversal forces, vertical load on the wheel and camber angle influence

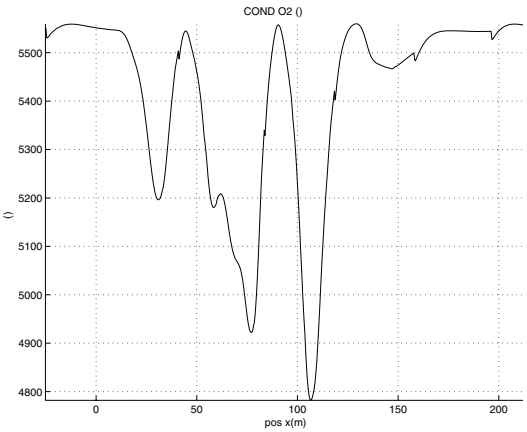

Fig. 8. Condition number of observability matrix - double lane change (90km/h)

A. Singular value of the observability matrix $\mathcal{O}_2$

The observability matrix $\mathcal{O}_2$ has three real singular values: $\lambda_1 > \lambda_2 > \lambda_3$

Fig.9 shows the progression of these singular values for a double lane change at 90km/h.

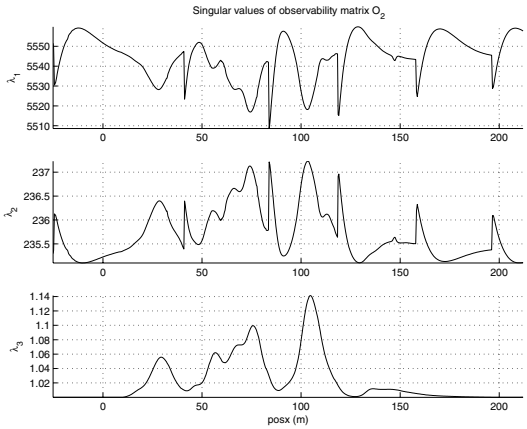

Fig. 9. Singular values of the observability matrix - double lane change (90km/h)

When computing is done with different paths (several speeds), the main values of λ_1 and λ_2 are directly linked to vehicle speed. But values of the smallest (λ_3) are always around 1. Variations in λ_3 are the same as the tire cornering stiffness reference given by the Callas simulator (Fig. 7).

B. Identification of tire cornering stiffness from the smallest singular value of the observability matrix

Because of the similarities between the shape of the smallest singular value of the observability matrix and "real"

tire cornering stiffness, a linear regression is performed to identify the parameters between both variables. A linear dependency is formulated as:

$$\begin{cases} 1/(C^1_{F\delta}) &= a_1\lambda_3(\mathcal{O}_2) + a_2 & (12a) \\ 1/(C^2_{F\delta}) &= b_1\lambda_3(\mathcal{O}_2) + b_2 & (12b) \end{cases}$$

To estimate parameters a_1, a_2, b_1 and b_2, a least-mean-square procedure was performed. The problem is to find θ_1 and θ_2, solutions of:

$$\mathbf{\Gamma}_1\theta_\mathbf{j} = \nu_\mathbf{j} \ ; \ \mathbf{j} = \{1;2\} \quad (13)$$

with $\theta_\mathbf{1} = \begin{pmatrix} a_1 \\ a_2 \end{pmatrix}$ and $\theta_2 = \begin{pmatrix} b_1 \\ b_2 \end{pmatrix}$.

There are n data samples. Least-mean-square matrices and vectors are written as:

$$\mathbf{\Gamma}_1 = \begin{pmatrix} (\lambda_3(\mathcal{O}_2))_1 & 1 \\ (\lambda_3(\mathcal{O}_2))_2 & 1 \\ \cdots & \\ (\lambda_3(\mathcal{O}_2))_n & 1 \end{pmatrix} \text{ and } \nu_\mathbf{j} = \begin{pmatrix} 1/(C^{j\ Callas}_{F\delta})_1 \\ 1/(C^{j\ Callas}_{F\delta})_2 \\ \cdots \\ 1/(C^{j\ Callas}_{F\delta})_n \end{pmatrix}_{j=\{1;2\}}$$

Problem (13) is solved using (14).

$$\widehat{\theta_\mathbf{j}} = \left(\mathbf{\Gamma}_1^T\mathbf{\Gamma}_1\right)^{-1}\mathbf{\Gamma}_1^T\nu_\mathbf{j} \ ; \ \mathbf{j} = \{1;2\} \quad (14)$$

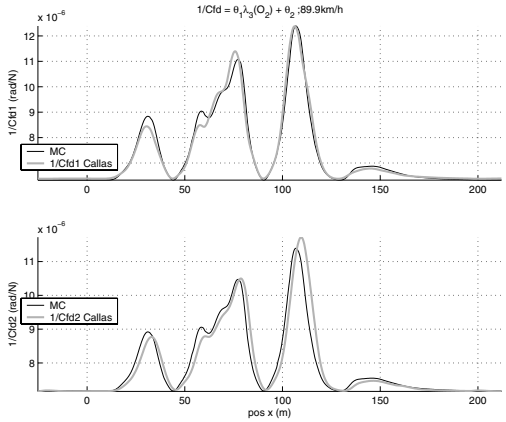

Fig. 10. First identification result - double lane-change (90km/h)

Fig. 10 shows the results of the first identification of tire cornering stiffness using the smallest singular value of $\mathcal{O}_2$ and (15) for a double lane change at 90km/h. Identification is quite good.

$$\begin{cases} 1/(\widehat{C^1_{F\delta}}) &= \hat{a}_1\lambda_3(\mathcal{O}_2) + \hat{a}_2 & (15a) \\ 1/(\widehat{C^2_{F\delta}}) &= \hat{b}_1\lambda_3(\mathcal{O}_2) + \hat{b}_2 & (15b) \end{cases}$$

The first identification procedure having been applied successfully in this test, other tests are performed on the same obstacle. The virtual vehicle performs the double lane change at eight different speeds : 40, 45, 50, 60, 70, 80, 90 and 105 km/h. The points in Fig. 11 correspond to results of this first identification procedure.

C. Identification of tire cornering stiffness from the smallest singular value of the observability matrix and vehicle speed

Because of the speed distribution of identified parameters ($\hat{a}_1$, $\hat{a}_2$ $\hat{b}_1$ and $\hat{b}_2$), the following relation is proposed:

$$\begin{cases} a_1 &= \left(a_{11}(V_G)^2 + a_{12}(V_G) + a_{13}\right) & (16a) \\ a_2 &= \left(a_{21}(V_G)^2 + a_{22}(V_G) + a_{23}\right) & (16b) \\ b_1 &= \left(b_{11}(V_G)^2 + b_{12}(V_G) + b_{13}\right) & (16c) \\ b_2 &= \left(b_{21}(V_G)^2 + b_{22}(V_G) + b_{23}\right) & (16d) \end{cases}$$

The different parameters of (16) are identified using a least-mean-square procedure.

$$\mathbf{\Gamma}_2\theta_\mathbf{j} = \nu_\mathbf{j} \ ; \ \mathbf{j} = \{3;4;5;6\} \quad (17)$$

with

$$\theta_3 = \begin{pmatrix} a_{11} \\ a_{12} \\ a_{13} \end{pmatrix}; \theta_4 = \begin{pmatrix} a_{21} \\ a_{22} \\ a_{23} \end{pmatrix}; \theta_5 = \begin{pmatrix} b_{11} \\ b_{12} \\ b_{13} \end{pmatrix}; \theta_6 = \begin{pmatrix} b_{21} \\ b_{22} \\ b_{23} \end{pmatrix}$$

$$\mathbf{\Gamma}_2 = \begin{pmatrix} (V_G)^2_1 & (V_G)_1 & 1 \\ (V_G)^2_2 & (V_G)_2 & 1 \\ \cdots & & \\ (V_G)^2_8 & (V_G)_8 & 1 \end{pmatrix}; \nu_\mathbf{j} = \begin{pmatrix} (\alpha_j)_1 \\ (\alpha_j)_2 \\ \cdots \\ (\alpha_j)_8 \end{pmatrix}_{\alpha_j=\{\hat{a}_1;\hat{a}_2;\hat{b}_1;\hat{b}_2\}}$$

Problem (16) is solved using:

$$\widehat{\theta_\mathbf{j}} = \left(\mathbf{\Gamma}_2^T\mathbf{\Gamma}_2\right)^{-1}\mathbf{\Gamma}_2^T\nu_\mathbf{j} \ ; \ \mathbf{j} = \{3;4;5;6\} \quad (18)$$

Results of the second identification procedure are schematized by continuous lines on Fig. 11.

The identification of tire cornering stiffness can be summarized by:

$$\begin{cases} 1/(\widehat{C^1_{F\delta}}) &= \left[\hat{a}_{11}(V_G)^2 + \hat{a}_{12}(V_G) + \hat{a}_{13}\right]\lambda_3(\mathcal{O}_2) \\ &\quad + \left[\hat{a}_{21}(V_G)^2 + \hat{a}_{22}(V_G) + \hat{a}_{23}\right] & (19a) \\ 1/(\widehat{C^2_{F\delta}}) &= \left[\hat{b}_{11}(V_G)^2 + \hat{b}_{12}(V_G) + \hat{b}_{13}\right]\lambda_3(\mathcal{O}_2) \\ &\quad + \left[\hat{b}_{21}(V_G)^2 + \hat{b}_{22}(V_G) + \hat{b}_{23}\right] & (19b) \end{cases}$$

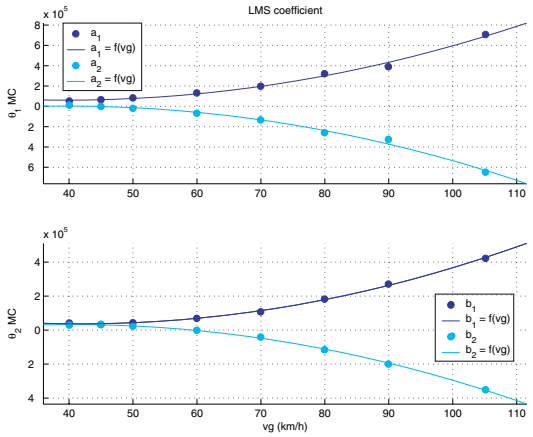

Fig. 11. Synthesis of identification result - double lane change at different speeds

D. Validation of the identified relation

The validation of parameter identification is done using the Callas simulator. The virtual driver carries out a slalom test at a constant speed of 60km/h. The steering wheel angle oscillates between -30 and 30 degrees, its frequency begins at 0.001Hz and finishes at 1Hz.

The slalom is a classical test to evaluate the lateral behavior of a vehicle. It is also a good test to determine relationship between roll, yaw and lateral movement of a car in response to the steering wheel input. During this test the vehicle displays a significant rolling movement. This implies large variations in lateral tire forces.

Fig. 12 shows the result of tire cornering identification applying (19) with the parameters identified from the eight double lane-change tests (cf section VI-C).

The relation was checked using a different type of test from that used for parameter identification, and the results were entirely convincing.

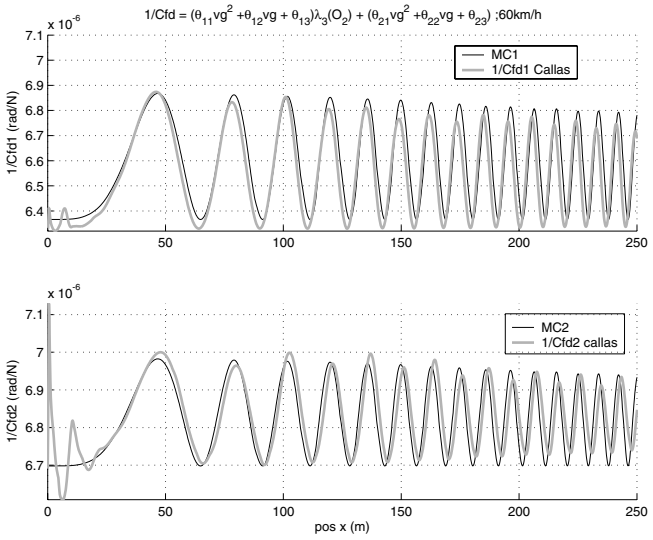

Fig. 12. Second identification validation - slalom (60km/h)

VII. CONCLUSIONS AND FUTURE WORKS

A. Conclusions

After having presented a nonlinear vehicle model, this paper has proposed a sliding mode observer of vehicle sideslip angle. This observer was validated on experimental data acquired with the Heudiasyc Laboratory experimental vehicle. By studying the observability properties of the observer, the paper has presented the relation between the observability matrix condition number and tire cornering stiffness variations obtained using a realistic vehicle simulator, Callas, developed by SERA-CD. A singular value decomposition of the observability matrix was performed, and the particular relation between variations in the smallest singular value and variations in the real tire cornering stiffness was highlighted.

As it has been shown in this paper, it is possible to identify the real tire cornering stiffness from the smallest singular value of observability matrix defined by a nonlinear vehicle model and a sliding mode observer. The identification procedure was done using several double lane-change tests and identified parameters were validated using a slalom test.

Some reservations should, however, be expressed. With high lateral acceleration, at the limit of vehicle stability, the proposed observer is unable to perform a good state reconstruction. Because the observability matrix is evaluated at the current observed state, the tire cornering stiffness cannot be computed satisfactorily.

B. Future Works

Future works will concern a more theoretical study of the observability matrix properties for parameter identification. The main limitations of the observer and consequently of tire cornering stiffness identification are directly due to the assumption concerning the linearity of tire-road transversal forces. Our next study will therefore examine an observer based on a vehicle model using nonlinear tire modeling, and the properties of the associated observability matrix.

VIII. NOTATIONS

$C_{F\delta}^{1,2}$ Front, rear wheel cornering stiffness $(N.rad^{-1})$
$F_l^{1,2}$ Longitudinal force in the front, rear wheel frame (N)
$F_t^{1,2}$ Transversal force in the front, rear wheel frame (N)
$L^{1,2}$ CG to front, rear axle distance (m)
V_G Speed of center of gravity $(m.s^{-1})$
β Steering angle (rad)
δ Vehicle sideslip angle (rad)
$\delta^{1,2}$ Front, rear wheel sideslip angle (rad)
$\dot{\psi}$ Yaw rate $(rad.s^{-1})$
$\{x\}_m$ measurement from sensor

REFERENCES

[1] S. Mammar and D. Koenig, "Vehicle handling improvment by active steering," *Vehicle system dynamics*, vol. 38, pp. 211–242, 2002.

[2] U. Kiencke and L. Nielsen, *Automotive control system*. Springer, 2000.

[3] P. Venhovens and K. Naab, "Vehicle dynamics estimation using kalman filters," *Vehicle System Dynamics*, vol. 32, pp. 171–184, 1999.

[4] H. Nijmeijer and A. J. Van der Schaft, *Nonlinear Dynamical Control Systems*. Springer-Verlag, 1990.

[5] J. Stéphant, "Contribution à l'étude et à la validation expérimentale d'observateurs appliqués à la dynamique du véhicule," Ph.D. dissertation, Université de Technologie de Compiègne, Décembre 2004.

[6] J. Stéphant, A. Charara, and D. Meizel, "Evaluation of sliding mode observer for vehicle sideslip angle," in *Proc. 16th IFAC World Congress*, july 2005.

[7] E. Busvelle and J.-P. Gauthier, "Observation and identification tools for nonlinear systems. application to a fluid catalytic cracker." *To appear in International Journal of Control*.

[8] M. Segel, "Theorical prediction and experimental substantiation of the response of the automobile to steering control," *Proc. automobile division of the institut of mechanical engineers*, vol. 7, 1956.

[9] D. Lechner, "Analyse du comportement dynamique des véhicules routiers légers : développement d'une méthodologie appliquée à la sécurité primaire," Ph.D. dissertation, École centrale de Lyon, Octobre 2001.

[10] W. Perruquetti and J.-P. Barbot, *Sliding mode control in engineering*. Marcel Dekker, Inc., 2002.

[11] H. B. Pacejka, *Tyre and vehicle dynamics*. Elsevier Butterworth-Heinemann, 2002.